Response of a Global Coupled Ocean–Atmosphere–Sea Ice Climate Model to an Imposed North Atlantic High-Latitude Freshening

WENJU CAI, JOZEF SYKTUS, HAL B. GORDON, AND SIOBHAN O'FARRELL

CSIRO Division of Atmospheric Research, Aspendale, Victoria, Australia

(Manuscript received 2 February 1996, in final form 9 July 1996)

ABSTRACT

The response of a coupled oceanic–atmospheric–sea ice climate model to an imposed North Atlantic high-latitude freshening is examined. The imposed freshening lasts for 5 yr with a total salt deficit equivalent to about eight times the observed Great Salinity Anomaly during the late 1960s and early 1970s.

The thermohaline circulation associated with North Atlantic Deep Water Formation (NADWF) initially weakens, but it recovers within 20 yr of the imposed freshening being removed. The effect of the weakened NADWF is gradually transmitted from high latitudes to the entire Atlantic Ocean. The response at the equator lags that at 62°N by about 10 yr. In the midlatitude (from 30° to 58°N) region, the lag causes a warming during the initial weakening and a cooling during the recovery. Changes in the thermohaline circulation significantly modify the large-scale North Atlantic circulation. In particular, the barotropic Gulf Stream weakens by about 18%.

An interesting feature is the dipole structure of the initial response in sea surface temperature, with cooling in the sinking region and warming south of it. This dipole structure plays an important role for the recovery of the NADWF once the imposed freshening is removed. It increases the surface density in the sinking region and increases the north–south pressure gradient. Thus, the conditions set up during the initial weakening contribute to the recovery process.

Modifications of the thermal structure of the ocean surface lead to changes in the atmospheric circulation, in particular, a weakening of the westerlies over the midlatitude North Atlantic and a southward shift over Western Europe. The North Atlantic oscillation (NAO) index under the imposed freshening is negative, consistent with findings from observational studies. The associated climate changes are similar to those observed with negative NAO values.

Effects of various oceanic and atmospheric feedbacks are discussed. The results are also compared with those from ocean-only models, where the atmosphere–ocean interactions and some of the oceanic feedbacks are excluded.

1. Introduction

A distinctive feature of the present-day coupled oceanic–atmospheric–sea ice climate system is that, in the high-latitude North Atlantic Ocean, the buoyancy loss through cooling exceeds the buoyancy gain through excess precipitation. This causes a sinking to deeper levels, an equatorward flow at depth, and a poleward motion near the surface, together known as North Atlantic Deep Water Formation (NADWF). Over the last decade, numerous studies have highlighted the importance of NADWF in maintaining the current climate (Broecker et al. 1985; Broecker 1991; Gordon 1986; Semtner and Chervin 1988; Manabe and Stouffer 1988). Its importance has inspired a large number of studies on the stability of NADWF to a high-latitude freshening in ocean-only models without a sea ice model (e.g., Bryan 1986; Wright and Stocker 1991; Power et al. 1994; Cai and Godfrey 1995; Rahmstorf and Willebrand 1995; Cai 1996). Typically, the model stability is compared to the observed response of the real ocean to the Great Salinity Anomaly (GSA). The GSA was a large freshening of surface water of the North Atlantic during 1968–72 (Dickson et al. 1988), which is believed to have been initiated by an anomalous outflux of sea-ice from the Arctic (Walsh and Chapman 1990). These model studies produced very different conclusions. Some suggest that NADWF is very unstable, while others indicate that it is extremely stable.

In the present study, we examine the stability of NADWF to a high-latitude freshening in a coupled system. Compared with ocean-only models, the coupled model includes many more oceanic feedback processes and allows ocean atmosphere interactions. The imposed freshening has a magnitude of salt deficit eight times that associated with the observed GSA. Several recent coupled model studies on a similar topic are most relevant. Manabe and Stouffer (1995) simulated abrupt climate change induced by freshwater input to the North

Corresponding author address: Dr. Wenju Cai, Division of Atmospheric Research, CSIRO, Private Bag 1, Mordialloc, Victoria 3195, Australia.
E-mail: wjc@dar.csiro.au

Atlantic Ocean. In their study, the discharge of freshwater is much larger and is imposed over a broader area. The freshwater flux anomaly is comparable to the rate of the pre-Younger Dryas of meltwater into the World Oceans. They were able to reproduce episodes that resemble the abrupt change of the ocean–atmosphere system recorded in ice and deep ocean cores (Keigwin and Jones 1994). They found that even under such a large anomalous freshening NADWF recovers by the end of the 300-yr integration. Nakamura et al. (1994) employed a simple coupled box model to explore the ocean–atmosphere interactions. They discovered several important feedbacks, including a positive one between eddy moisture transport (ETM) and the thermohaline circulation, and examined the importance of these feedbacks in determining the stability of NADWF. This work is continued by Saravanan and McWilliams (1995) in an idealized coupled model. We will explore the effect of these feedbacks in our coupled model.

In reality, the response of NADWF to a freshening is determined by several major oceanic feedbacks between the thermohaline circulation and the high-latitude temperature and salinity, which have opposing effects on density, and by feedbacks between atmospheric transports and the thermohaline circulation. Let us consider a negative anomaly in the strength of the thermohaline circulation due to a freshening. The anomaly may induce the following simultaneous processes.

1) A positive feedback between overturning and surface salinity (Stommel 1961). The negative anomaly transports less salt northward and reduces high-latitude surface salinity and hence lowers the surface density there. This low density in turn weakens the deep water formation and the overturning circulation.
2) A negative feedback between overturning and surface temperature. As the overturning circulation decreases, the associated weakened northward heat transport lowers high-latitude surface temperature and raises surface density there. The high density in turn strengthens convective activity and hence thermohaline circulation.
3) A positive feedback between overturning and evaporation. Evaporation decreases when the weakened thermohaline circulation leads to lower surface temperature. If this decrease is not compensated for by a commensurate decrease in precipitation, surface salinity and surface density will decrease. This will in turn lead to a weaker overturning circulation and a further decrease in evaporation. This is called EMT feedback by Nakamura et al. (1994). It is a positive feedback between moisture transport and the thermohaline circulation, because as overturning weakens, high-latitude temperature decreases. This causes the meridional temperature gradient to increase, leading to an increased poleward atmospheric moisture transport, further decreasing the overturning.
4) A negative feedback between overturning and ice melting/formation. As the overturning circulation decreases, the weaker northward heat transport lowers the polar surface temperature. This leads to increased ice formation. The associated brine rejection increases density, strengthening the overturning circulation.
5) A positive feedback between albedo and high-latitude atmospheric temperature. As the atmospheric temperature cools, and as more sea ice forms, cloud cover increases. As a result, surface and planetary albedo increase, further decreasing the atmospheric temperature. Since low atmospheric temperature tends to cool the SST, which in turn favors high-latitude sinking, this feedback acts to stabilize the thermohaline circulation. Therefore one may regard this mechanism as a negative feedback between albedo and overturning.
6) A positive feedback between atmospheric heat transport and the thermohaline circulation. This feedback operates because the sum of the atmospheric and oceanic heat transport—that is, the net heat into the coupled system—is nearly constant, despite feedback 5. This ''near constancy'' means that as the high-latitude sinking becomes weaker the poleward atmospheric heat transport increases, which tends to warm the high latitudes and weaken the high-latitude sinking further.

We show that in the presence of these processes initial anomalies associated with an imposed freshening exert impacts in areas remote from the freshening region, influencing the atmospheric circulation and regional climate. We discuss the atmosphere–ocean interactions, and how they in turn modify the oceanic circulation.

An ocean-only model usually presents only a limited number of processes. Under traditional mixed boundary conditions, forcing for salinity is provided by a fixed flux and the forcing for the temperature is provided by a heat flux parameterized via Haney's (1971) restoration scheme. NADWF is extremely sensitive to a high-latitude freshening (e.g., Bryan 1986; Wright and Stocker 1991; Power et al. 1994). This is because Haney condition usually uses a thermal damping rate of 30–50 W m^{-2} s^{-1}. This means that feedback 2 is very limited and that the SST is strongly constrained and is not allowed to move much away from the restoring temperature. With a fixed flux for salinity and without a sea-ice model all the other processes are eliminated except for feedbacks 1 and 6. Under this set of boundary conditions, feedback 6 is implicit and extremely strong; it implies that the atmospheric heat transport responds to changes in heat flux to keep the SST nearly constant. This positive feedback is partially responsible for the high sensitivity of the NADWF under this set of boundary conditions. Yang and Neelin (1993) and Zhang et al. (1995) included an ice model and found that the thermohaline circulation is more stable than otherwise. Some recent

studies (e.g., Cai and Godfrey 1995; Cai 1996; Rahmstorf and Willebrand 1995) have used modified mixed boundary conditions, in which, although a fixed flux for salinity is used, the heat flux is parameterized via a more realistic scheme, which allows feedback 2. These studies found that the model NADWF is very stable.

It follows that ocean-only models may not be capable of properly representing the relative importance of these processes. For example, it is not clear how feedback 3 may be incorporated. Indeed, to date, none of the ocean-only models includes this feedback. Further, the relative importance of each process varies with time and space, and representing this in ocean-only models is extremely difficult. These arguments reinforce the need for a fully coupled model in order to properly examine the stability of NADWF. The coupled oceanic–atmospheric–ice model used in this study has the advantage over early ocean-only studies in that all the feedbacks are present; their strengths are time and scale dependent and are responsive to the dynamics of the coupled system.

The structure of the rest of this paper is as follows. In section 2 we briefly describe the coupled model, possible effects of flux corrections, and the experimental procedure. In sections 3 and 4 we describe the response of the system. In section 5 we present a summary.

2. The coupled model and the imposed high-latitude freshening

a. The coupled model

A detailed description of the CSIRO global coupled model is given by Gordon and O'Farrell (1997). It consists of atmospheric, oceanic, sea-ice, and biospheric components and has full annual and diurnal cycles. The spectral, nine-level, atmospheric general circulation (GCM) model is an updated version of CSIRO9 AGCM described by McGregor et al. (1993), Watterson et al. (1995), and Hunt et al. (1995). The gridpoint, 12-level, oceanic GCM is a version of the Geophysical Fluid Dynamics Laboratory model based on Bryan (1969) and is described in detail by Moore and Reason (1993) and Moore and Gordon (1994). The coupled model horizontal resolution is that of the spectral atmospheric GCM (R21), which gives a grid resolution of about 5.6° long × 3.2° lat. The temperature–salinity grid points of the oceanic GCM are coincident with the spectral transform grid points of the atmospheric GCM. The ice model is dynamic and includes the cavitating fluid rheology of Flato and Hibler (1990). The thermodynamic part employs a three-level form (Semtner 1976), which allows for internal heat capacity in the ice. The ice concentration and the percentage of open water are determined from the energy budget of the mixed layer adjacent to the ice in the partially covered grid box. Both vertical and lateral accretion/ablation of ice are accounted for. Unlike many other GCMs, the ice model is incorporated as part of the atmospheric GCM, not the oceanic. A full description of the ice model and its behavior is given by O'Farrell (1997, manuscript submitted to *J. Geophys. Res.*). Land surface interactions are parameterized using a soil-canopy model (Kowalczyk et al. 1991, 1994).

The atmospheric GCM uses a time step of 30 min, while the oceanic GCM has a time step of 60 min. The coupled model is run synchronously, with one oceanic time step being followed by two atmospheric steps. The atmospheric fluxes are averaged over the two steps and passed to the oceanic model. The coupled model uses corrections to the quantities through which the atmospheric and oceanic GCMs are coupled (here the term ''atmospheric GCM'' refers to the atmospheric–ice–biospheric model). The method of correcting fluxes is described in Gordon and O'Farrell (1997). In this version of the coupled model, corrections applied to the atmospheric GCM-generated surface heat flux, salinity forcing (which consists of precipitation minus evaporation, land runoff, and sea-ice brine rejection/uptake), and surface stresses. Additional corrections are also applied to the oceanic GCM-generated surface temperature and salinity in order to further reduce climate drift (see Gordon and O'Farrell 1997). These corrections are diagnosed from precoupling spinups to the climatologies of Levitus (1982) and using the surface wind stress of Hellerman and Rosenstein (1983). The corrections are kept constant (with a seasonal cycle) in subsequent coupled model experiments described in this paper. As in other coupled models (e.g., Manabe and Stouffer 1993, 1994, 1995), these corrections are necessary to prevent the rapid drift of the model state from the realistic precoupling spinups.

b. Possible effects of flux corrections

A question arises as to whether these flux corrections significantly affect the system's response to an external perturbation. On the one hand, Manabe and Stouffer (1995) noted that because the corrections are determined before the time integration of the coupled model and are not correlated to the transient surface anomalies of temperature and salinity, which can develop during the integration, they are unlikely to either systematically amplify or damp the anomaly. On the other hand, the state-of-the-art coupled models have many major errors. These include very poor simulations of atmospheric heat transports and heat flux by the atmospheric GCMs (Glecker et al. 1995), and very poor simulations of convection by oceanic GCMs (Danabasoglu and McWilliams 1995). There are increasing numbers of studies exploring the possible effects of flux corrections (Nakamura et al. 1994; Marotzke and Stone 1995; Schneider 1996; Cai and Chu 1996). Nakamura et al. (1994) argued that when these errors are large they may cause the atmosphere–ocean interactions to be distorted. In their simplified coupled system, which they adopted as the ''real world,'' they artificially introduced an error to

create the ''model world.'' They then corrected the error through a flux adjustment so that the model world has an identical solution to the real world. They found that the sensitivity to a salt perturbation of the real world differs significantly from that of the corrected model world. The errors in their model were due to the fact that the model errors are associated with processes that have feedbacks. They argued that the conventional flux corrections can give only the right sensitivity if there are no feedbacks associated with the enroneous processes. Cai and Chu (1996) argued that since flux corrections are diagnosed from precoupling spinups, any incompatibility between the model dynamics and the climatology, to which the model oceanic surface field is restored, can be carried over to the coupled system. During the spinup the surface climatology of the model ocean is forcefully ''nudged'' toward that of a climatology, regardless of whether or not the internal dynamics of the model ocean can maintain the climatology. This leads to intermittent convections in the spinup state. When the saline and thermal dampings become weaker, as is the case when coupling occurs, the system chooses convective pattern (the location and intensity of the convection) more compatible with the internal dynamics. They argued that in the permanent presence of such an incompatibility the system's response to external perturbation may be contaminated. The work Danabasoglu and McWilliams (1995) also points to the problem of poor simulation of convection. These results are highly relevant to the present study and add caveats in interpreting results derived from flux-corrected coupled models. We note, however, that while the flux corrections do not eliminate the errors of the model dynamics, they do prevent the rapid drift of the model state from the realistic precoupling spinup, which could more seriously distort the model results of a numerical experiment.

As already discussed above, one of the principal questions is whether the errors that lead to climate drift and the need for flux corrections will cause errors in model sensitivity to perturbations. We have attempted to evaluate the effect of poleward heat transport associated with the flux corrections on feedbacks 1–6. A comparison between implied heat transports with and without heat flux corrections shows that, without the heat flux correction, the oceanic heat transport is unrealistic from 30°N southward, similar to many other models (see Gleckler et al. 1995). The maximum in the Southern Hemisphere is only about 0.5 PW and the transport is northward from 10°S to the equator, with a northward heat transport of about 1.2 PW across the equator. In the latitude band from 30° to 70°N, the heat transport is better in both magnitude and direction; although the magnitude is generally about 0.3 PW smaller than that without flux correction. As results of the above features, the implied correction in heat transport is large 30°N southward but small from 30°N northward with a maximum correction of less than 0.4 PW. We are interested

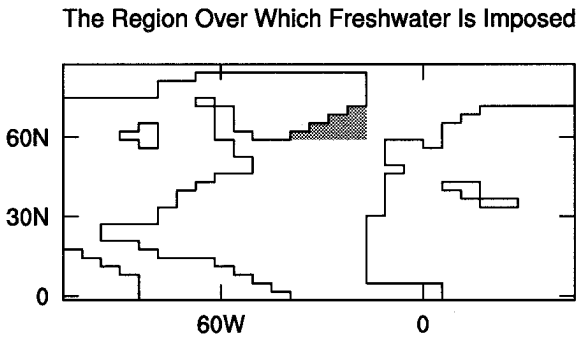

FIG. 1. The region over which the freshwater (equivalent salt flux) is imposed.

in the North Atlantic region from 30° to 70°N. At these latitudes, the flux correction increases the heat transport and acts to intensify feedbacks 2–4. However, since feedbacks 2 and 3 are negative ones, whereas feedback 4 is a positive one, it is not clear whether the changes on balance increase or decrease the stability of the thermohaline circulation associated with NADWF.

We have also attempted to evaluate the influence of the use of flux corrections on simulations of climate. Although not in the direct context of the present study, the following results are worth noting. Comparisons between results using the CSIRO9 flux-corrected coupled model and using the CSIRO4 atmospheric GCM coupled to a dynamic upper-ocean model without flux correction (Syktus et al. 1994; Chappell and Syktus 1996) in simulations of paleoclimates at 6, 116, and 126 ka (thousand years) BP show that broad regional features simulated by these two different models are similar—that is, both models are able to simulate glacial initiation at 116 ka BP, with a comparable extent of perennial snow cover, an enhanced Northern Hemisphere summer monsoon at 126 and 6 ka BP, and a greatly reduced summer monsoon at 116 ka BP. In addition, both models simulate well the location and magnitude of precipitation changes. Thus, it would appear that flux corrections in the CSIRO9 flux-corrected coupled model do not have a significant effect on simulated climate.

c. The imposed high-latitude freshening

Negative salt flux anomalies are applied to the small region of the North Atlantic shown shaded in Fig. 1. This area is chosen to be almost the same as in Power et al. (1994) and Cai (1996). The salt deficit of the 1968–82 GSA was estimated by Dickson et al. (1988) to be 7.2×10^{13} kg. The experiment here, however, is not an attempt to simulate the actual GSA, but to examine the response of the coupled system to a freshening in the same part of the oceans. The salt anomalies are imposed for 5 yr and are in total equivalent to about eight times the observed salt deficit associated with the observed GSA. This amount of freshening has been used in the ocean-only model experiments of Power et al. (1994),

Cai (1996), and Rahmstorf and Willebrand (1995), and allows for an intercomparison of model responses.

As in other coupled models, some drift from precoupling spinup states takes place upon coupling. To reduce the interference of these drifts, the coupled model is run for 191 yr before the anomalies are imposed. By this time, the climate drift had reduced considerably. In the first century of the coupled model control run, the temperature drift in the global mean surface temperature was -0.4°C, while in the second century it was only -0.1°C. Hereafter, two cases are run. In one, the coupled model continues, and this is referred to as the control run. In another, the salt anomalies are applied at the beginning of year 192, and this run is referred to as the GSA experiment. The anomalies are applied for 5 yr and stop abruptly at the end of year 196; the GSA experiment was run for 51 yr in total.

3. The response during the imposed freshening

The coupled model exhibits strong seasonal signals. Superimposed on the seasonal signals are those that are weaker and of longer timescales, such as interannual, interpentadal, and interdecadal variabilities. Since we are interested in longer timescale signals, seasonal ones are filtered out and only annual mean results are presented, unless stated otherwise.

The ocean state prior to the anomalies is summarized in Fig. 2. The North Atlantic overturning (Fig. 2a) has a predominant NADWF cell, and a northern intrusion cell from the Southern Hemisphere, although the former is possibly too strong [with a magnitude of about 20 Sv (Sv = 10^6 m^3 s^{-1})]. The global overturning (Fig. 2b) features major overturning cells such as the Deacon cell, the Antarctic Circumpolar Convective cell, and the northern intrusion cell, as well as the NADWF. The global and Atlantic poleward heat transport (Fig. 2c) has magnitudes within commonly obtained ranges. The northward heat transport at most of the latitudes of the Atlantic Ocean reflects the model conveyor belt circulation associated with NADWF (Broecker et al. 1985). An examination of the model baroclinic circulation shows that the NADWF is compensated mostly via a path whereby water leaving the Atlantic returns through the Drake Passage with the Antarctic Circumpolar Current (ACC) cold water (Rintoul 1991; Cai 1994; Cai and Greatbatch 1995).

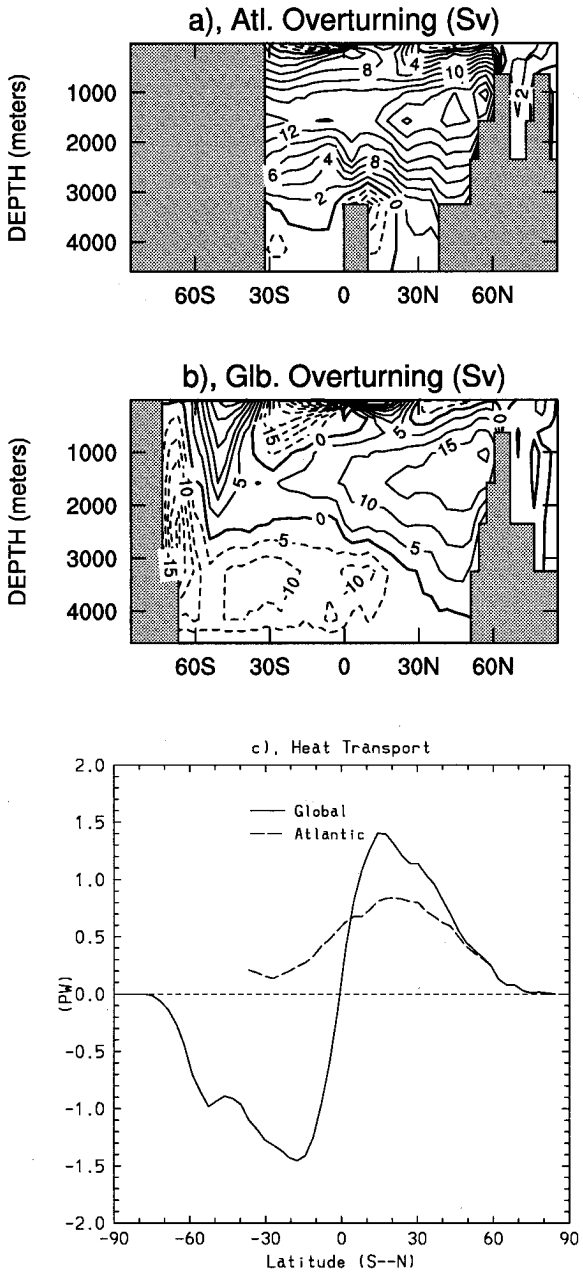

FIG. 2. The ocean state prior to the imposed freshening, (a) the overturning for the North Atlantic (Sv), (b) the overturning for the global ocean (Sv), and (c) the poleward heat transport for global and Atlantic Oceans (PW).

a. The weakening of NADWF

The time evolution of oceanic response in comparison with those of the control run is presented in Fig. 3. Figure 3a shows the model NADWF taken at a point where prior to the anomalies it is near a maximum. Figures 3b, 3c, and 3d show the Atlantic zonal mean of surface temperature, salinity, and density, respectively, at approximately 62°N, a latitude located at center of the area of imposed freshening. Despite the variabilities mentioned above, the impact of the freshening is clear. The NADWF weakens substantially, in sharp contrast to the control run, which remained within the range of a couple of Sv. As the freshening proceeds, high-latitude water becomes fresher and less dense. NADWF reaches a minimum of about 16 Sv [panel (i) of Fig. 4a] at year 197, about 1 yr after the imposed freshening is removed. By this time, negative temperature (potential), salinity, and density (potential) anom-

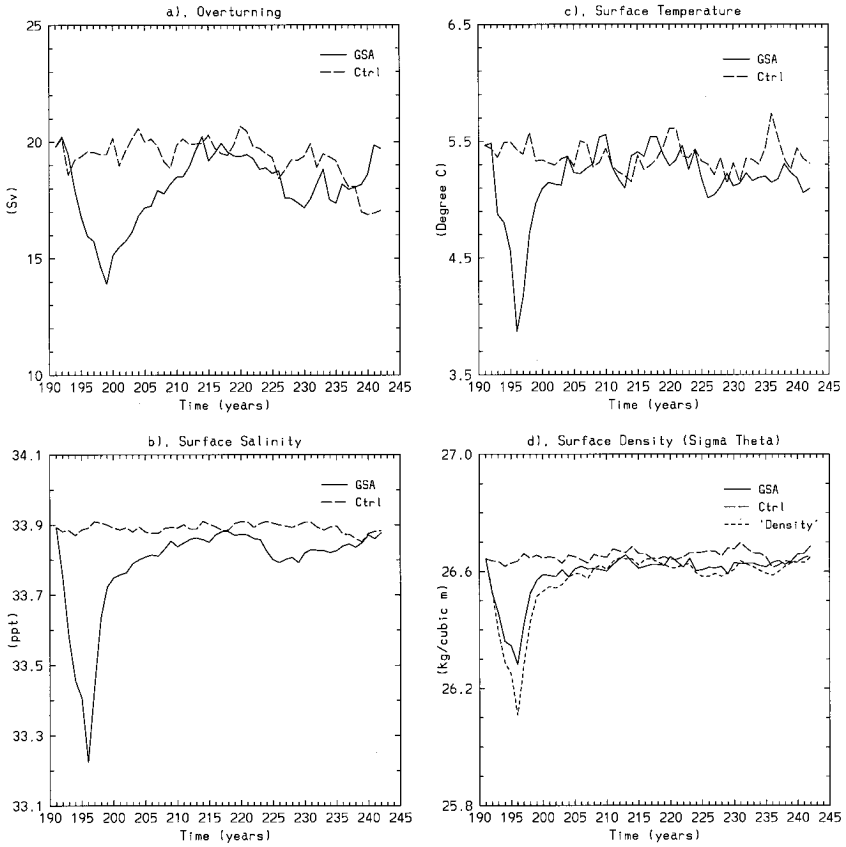

FIG. 3. Time evolutions of oceanic response in comparison with those of the control run. (a) The model NADWF taken at a point where prior to the anomalies it is near a maximum. (b), (c), and (d) Atlantic zonal mean surface temperature (°C), salinity (ppt), and density (σ_θ), respectively, at approximately 62°N, a latitude located at the center of the area of the imposed freshening. The fine dashed line shows the surface density calculated using the surface temperature of the control run and the salinity of the GSA experiment.

alies have developed at high latitudes and penetrated to depth [panel (i) of Figs. 4b–d].

The geographical distribution of the surface anomalies at different times is shown in Fig. 5. At year 197, south of the negative surface temperature and salinity anomalies, positive temperature and salinity anomalies develop. The positive temperature anomalies apparently dominate the salinity anomalies, leading to the low density from 30°N northward. The low density weakens the convective activity, and the convective mixed layer becomes shallower (Figs. 6a and 6b). Note that since convection in the North Atlantic mainly occurs in the northern winter results for this field are averages over the winter season rather than the entire year.

b. The feedbacks

The feedbacks between surface temperature and overturning, and between surface salinity and overturning are evident from Figs. 3b and 3c. In particular, the Atlantic zonal mean surface temperature drops by 1.3°C (see Fig. 3c). The positive feedback between evaporation–salinity and overturning (EMT feedback) can be seen from Figs. 7 and 8. Spatially, the change in evaporation (Fig. 7) correlates well with surface temperature [Fig. 5a(ii)]. Figure 8a shows the time series of the Atlantic zonal mean evaporation at 62°N. As the surface temperature drops, evaporation decreases. However, the change in evaporation is not compensated for by changes in precipitation. A time series of precipitation at the same latitude shows no significant difference between the GSA experiment and the control run, and the evaporation minus precipitation (E − P) field (figure not shown) indicates that it is dominated by the reduction in the evaporation rate in the region with imposed freshening. The associated EMT feedback operates with a well-defined increase in the atmospheric moisture transport (Fig. 8b), as can be seen from that at about 53°N. We choose this latitude because across this latitude the north–south gradient in evaporation is strongest (see Fig. 8). The negative feedback between sea ice melting/formation and overturning can be seen from Fig. 9. As the freshening proceeds, sea ice extends south to the region where the freshening is imposed and the

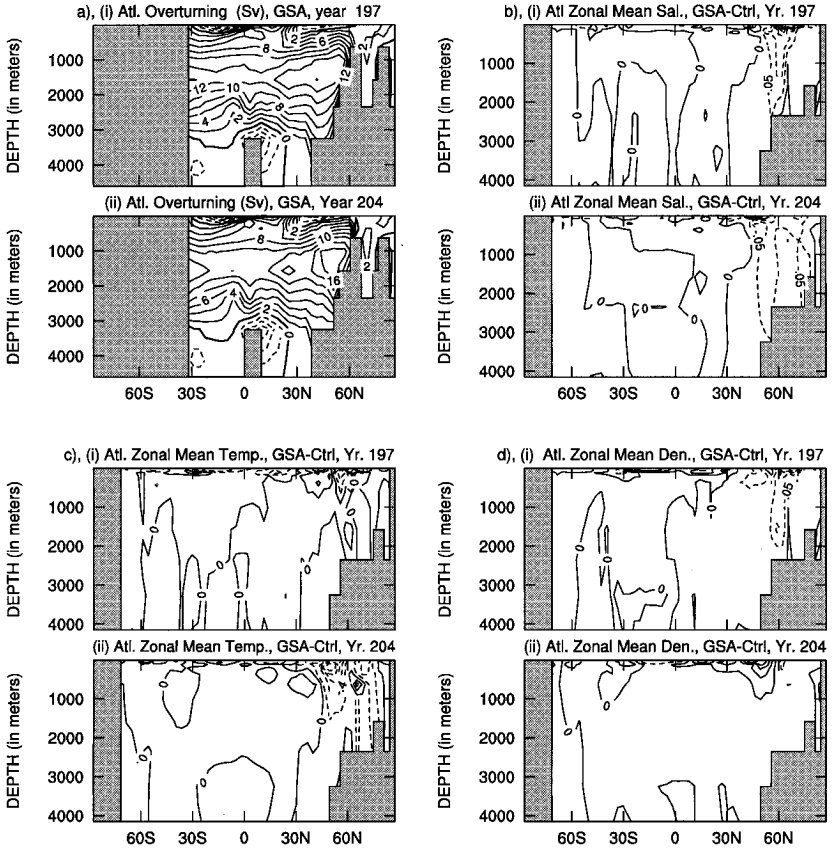

FIG. 4. Latitude–depth plot of (a) Atlantic overturning, and the difference (GSA experiment—control run) in the Atlantic, (b) zonal mean salinity, (c) zonal mean temperature, and (d) zonal mean potential density, at (i) year 197 and (ii) year 204.

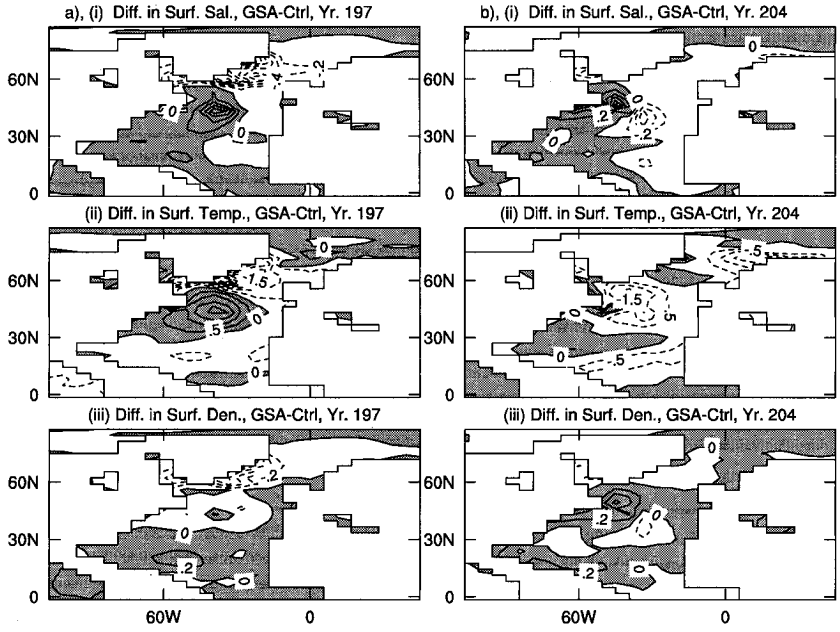

FIG. 5. Geographical distributions of the difference of surface fields (GSA experiment—control run) at (a) year 197 and (b) year 204 of (i) surface temperature, (ii) surface salinity, and (iii) surface density (σ_θ).

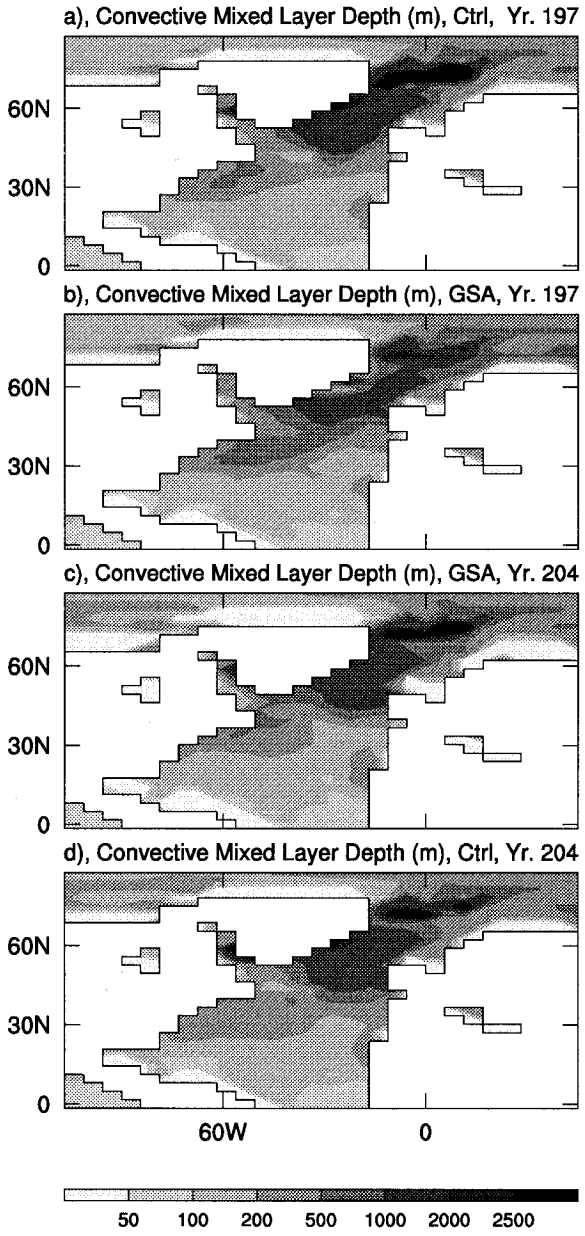

FIG. 6. Convection mixed layer (m) for the North Atlantic sector at (a) year 197 of the control run, (b) year 197 of the GSA experiment, (c) year 204 of the GSA experiment, and (d) year 204 of the control run. Since convection in the North Atlantic mainly occurs in the northern winter, results for this field are averages over the winter season rather than the entire year.

surface temperature drops. A plot of velocity of sea ice indicates increased southward transport of ice from Davis and Denmark Straits during the period from year 195 to year 199. The signal of increased sea ice thickness at a higher latitude is not as clear (related to temperature anomalies there; in the northern part of Greenland Sea and over most of the polar Arctic there are positive temperature anomalies; see section 3e). The associated brine rejection is expected to reduce the

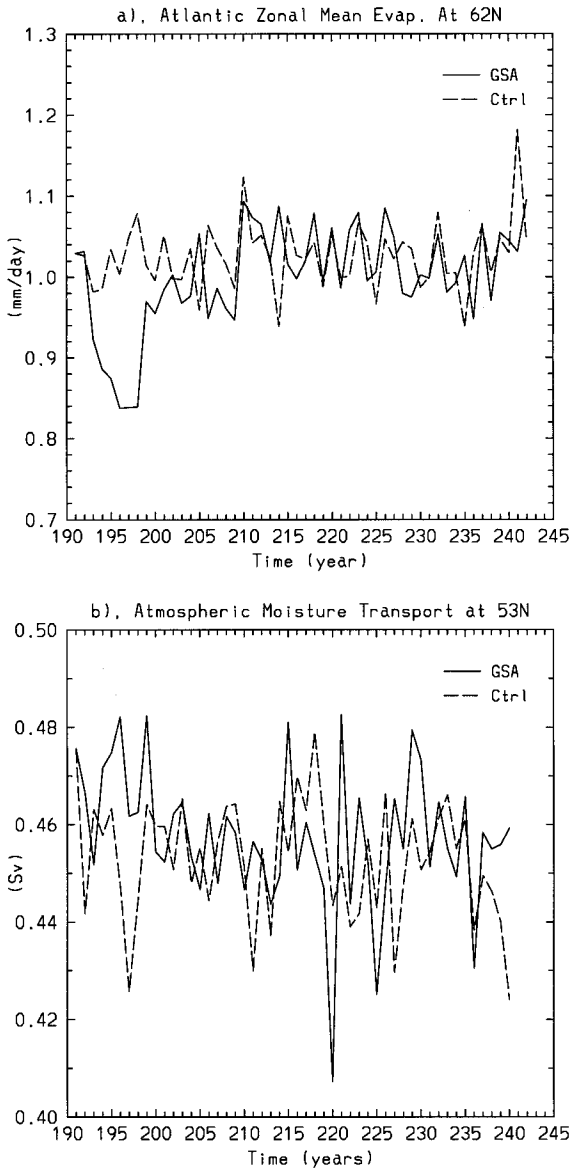

FIG. 7. Time series of Atlantic zonal mean (a) evaporation (mm day^{-1}) and (b) atmospheric moisture transport (Sv) at 53°N.

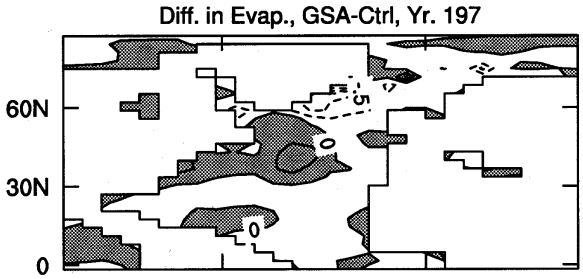

FIG. 8. Geographical distributions of the difference (GSA experiment—control run) in evaporation (mm day^{-1}) at year 197.

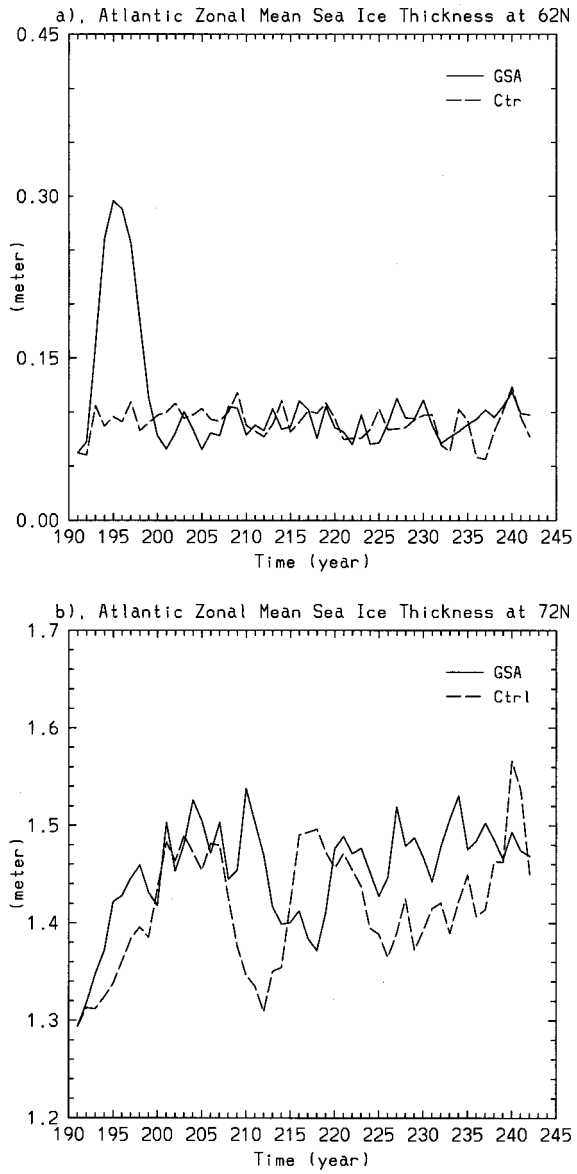

FIG. 9. Time series of Atlantic zonal mean sea ice thickness (m) at (a) 62°N and (b) 71°N.

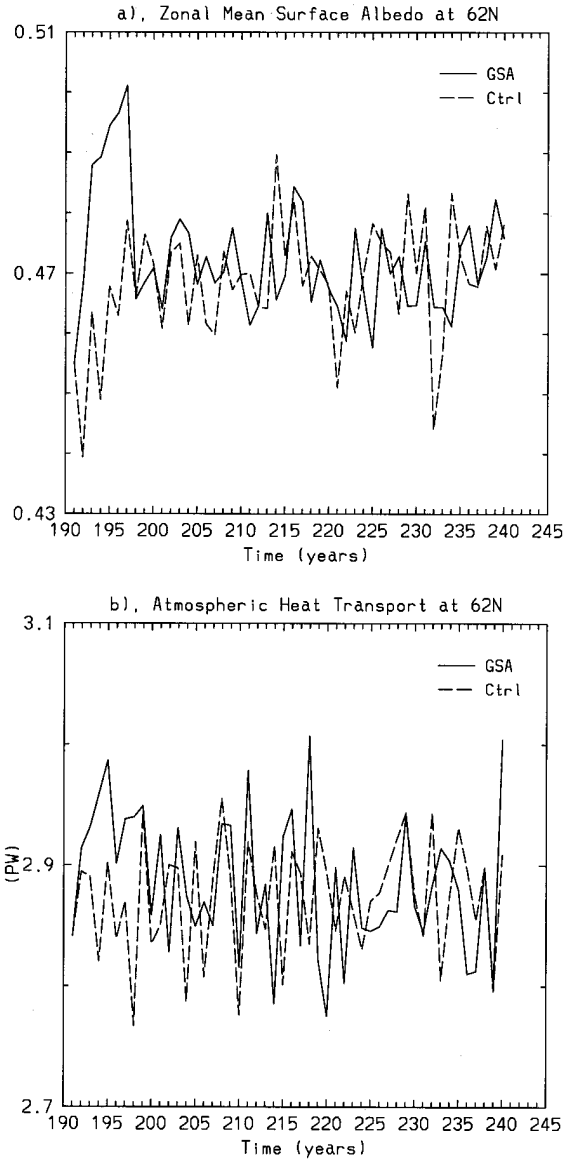

FIG. 10. Time series of (a) zonal mean surface albedo and (b) atmospheric heat transport, both at 62°N.

weakening of NADWF. As cooling and increase in sea ice occur, the feedback between albedo and temperature comes into play. Surface albedo at northern high latitudes increases (Fig. 10a), especially over the area of the imposed freshening. Increased high-latitude planetary albedo and total cloud cover, particularly the low cloud cover, are also seen, with a maximum over the region of the imposed freshening. As mentioned above, this process has the effect of stabilizing the overturning. Although local changes in planetary albedo take place, the amount of net heat entering from the top of the atmosphere into the coupled system hardly changes, implying a near constancy of the sum of the atmospheric and oceanic heat transport. As the NADWF weakens, and the oceanic heat transport decreases, the atmospheric heat transport increases to compensate for the decrease (Fig. 10b). This in turn has an effect of warming the ocean and thereby destabilizing the thermohaline circulation.

In the presence of all these feedbacks, the weakening of NADWF is less than that in the model of Power et al. (1994), which used mixed boundary conditions. In their model, NADWF reduces from about 22 to about 11 Sv when subject to an identical strength of perturbation. The larger weakening eventually led to a collapse of NADWF. As commented upon in section 1, under mixed boundary conditions the adjustment of surface temperature is curtailed, allowing mainly the pos-

itive feedback between surface salinity and overturning, and between the atmospheric heat transport and overturning. Indeed, in response to a decrease in salinity, surface temperature drops much less in their case than in our case (see their Fig. 7). Further, the temperature anomalies in their experiment are confined to the area of imposed freshening, and the impacts at lower latitudes are absent.

To get a feeling for the importance of the negative feedback between surface temperature and overturning and the positive feedback between the atmospheric heat transport and the overturning, the surface density has been computed using the surface salinity of the GSA experiment and the surface temperature of the control run. This somewhat mimics a situation in which temperature does not adjust, similar to that in the model under mixed boundary conditions. This implies that the feedback between temperature and overturning is disabled and the feedback between atmospheric heat transport and overturning is allowed to operate at an unrealistic strength. The time series is shown in Fig. 3d (fine-dashed line), the density would drop by a further 50%. This would further weaken NADWF, as was in the Power et al. (1994) study. It has been speculated (Tziperman 1994) that the high sensitivity under mixed boundary conditions is due to the unrealistic fixed freshwater flux. Cai (1996) shows that this is not the case. It is interesting, however, to note that even under such a situation, which strongly favors the destabilization of the overturning, the surface density recovers. This implies that the remaining negative feedbacks can play a significant role in stabilizing the thermohaline circulation.

The weakening of NADWF in the coupled model is much greater than in the ocean-only models of Rahmstorf and Willebrand (1995), Cai and Godfrey (1995), and Cai (1996), which allow only the feedbacks between surface temperature and overturning and between surface salinity and overturning. For example, in Rahmstorf and Willebrand's model, subject to the same amount of freshening, NADWF reduces by only 2 Sv. It was speculated that the stability of NADWF in these models is overestimated and that when the positive feedback between evaporation–salinity and overturning (EMT feedback) is included the stability would decrease (Willebrand 1993; Marotzke 1994; Nakamura et al. 1994). The results presented here support this point. Even in the presence of the negative feedback between sea ice dynamics and overturning, and between albedo and overturning, both of which act to increase the stability, NADWF in the coupled model weakens to a greater extent than in these models.

c. Large-scale oceanic circulation

Time series of the barotropic Gulf Stream at 27°N, 60°W and Kuroshio at 27°N, 160°E are presented in Figs. 11a and 11b. They show that the signal in the former is clear-cut but not so in the latter. The Gulf Stream weakens by about 5 Sv, which is about 18% of the initial magnitude. The minimum is reached at about year 203, which is at the same time as when the heat transport at this latitude is weakest (see section 3d). This suggests that this reduction results mainly from changes in the thermohaline circulation. The changes in the Kuroshio (figure not shown) are less well defined, and are probably due to the chaotic nature of the system.

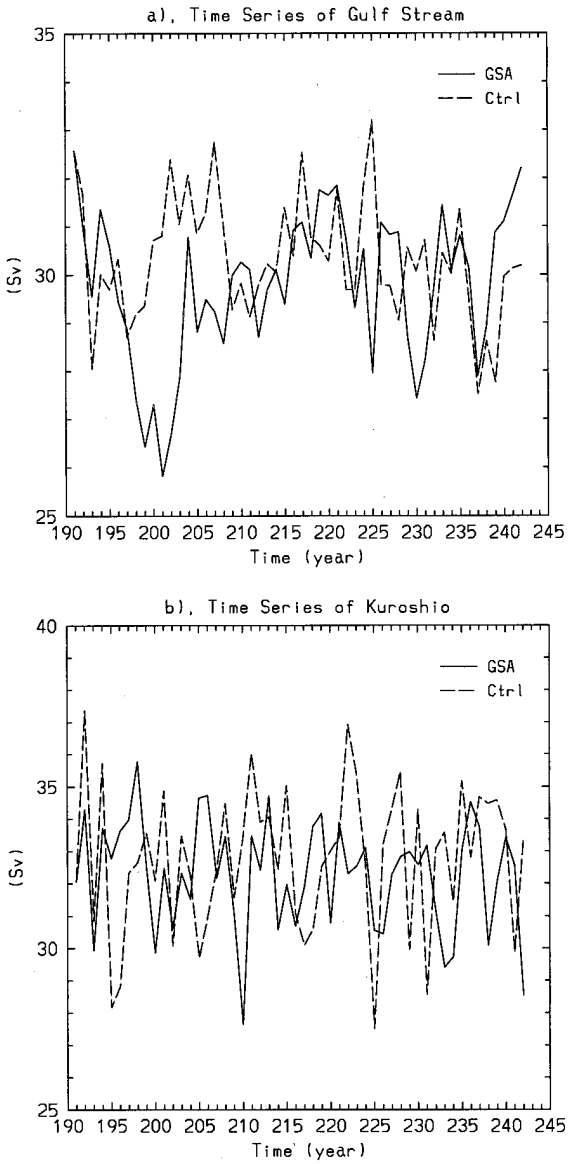

FIG. 11. Time series of the barotropic (a) Gulf Stream (Sv) at (27°N, 50°W) and (b) Kuroshio (Sv) at (27°N, 160°E).

The notion that the change in the Gulf Stream is mainly induced by changes in thermohaline circulation is supported by results of previous studies. Greatbatch et al. (1991) and Cai (1994) have demonstrated that about half of the Gulf Stream is thermohaline-driven

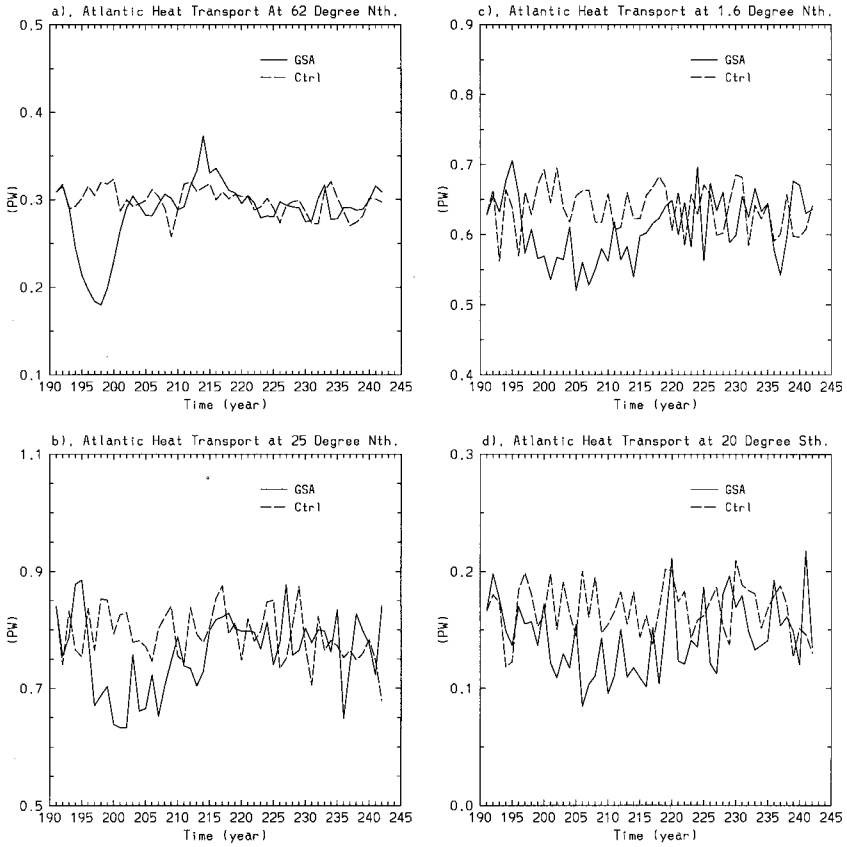

FIG. 12. Atlantic poleward heat transport at (a) 62°N, (b) 25°N, (c) 1.5°N, and (d) 20°S, respectively.

through the effect of the bottom pressure field (Holland 1973), in sharp contrast to the Kuroshio, which is mainly wind-driven (Cai 1994; Cai and Baines 1996). Greatbatch et al. found, on the basis of a diagnostic model driven by the Levitus (1989a, 1989b, and 1989c) datasets, that the Gulf Stream was up to 30 Sv weaker in the pentad of the early 1970s (between 1970 and 1974) than in that of the late 1950s (between 1955 and 1959) and that this difference was driven by the bottom pressure field. They speculated that weak convection in the period 1967–72 (during the GSA) may have been important for the change in transport they described. This is supported by the results presented here. Indeed, our results suggest that the largest change occurs somewhat later, and that Greatbatch et al.'s calculation for the pentad of 1970s may not coincide with the maximum response. In our model, because of the lag described above, convection has recovered by the time of the maximum Gulf Stream response. This time-lag between convection and the Gulf Stream, however, cannot be verified by the study by Greatbatch et al. (1991), because their study covers only 10 yr.

The large-scale baroclinic circulation associated with the conveyor belt circulation is modified considerably. The weakening of the overturning circulation reduces the poleward advection of the low-latitude water. Consequently, poleward surface flows and southward deep water outflow are generally weakened.

d. Poleward heat transport and heat budget

The freshening and its response induced modifications to the poleward heat transport and heat budget of the entire North Atlantic Ocean. Time series of the heat transport at different latitudes are presented in Fig. 12. At 62°N, the heat transport drops by about 0.12 PW. This drop is compensated by a commensurate increase in the atmospheric heat transport (Fig. 10b), although the atmospheric heat transport fluctuates more vigorously. This further confirmed the fundamental characteristics of the coupled system that the sum of the atmospheric and the oceanic heat transport is nearly constant (Stone 1978; Nakamura et al. 1994; Saravanan and McWilliams 1995), reinforcing that there exists a strong negative feedback between the atmospheric and oceanic heat transport. A plot of the difference in these two fields between the GSA experiment and the control run shows that such a compensation takes place at all latitudes.

An interesting feature is that the response of the oceanic heat transport (hence also the atmospheric heat transport) at lower latitudes lags that at higher latitudes. For example, poleward heat transport at 62°N reaches

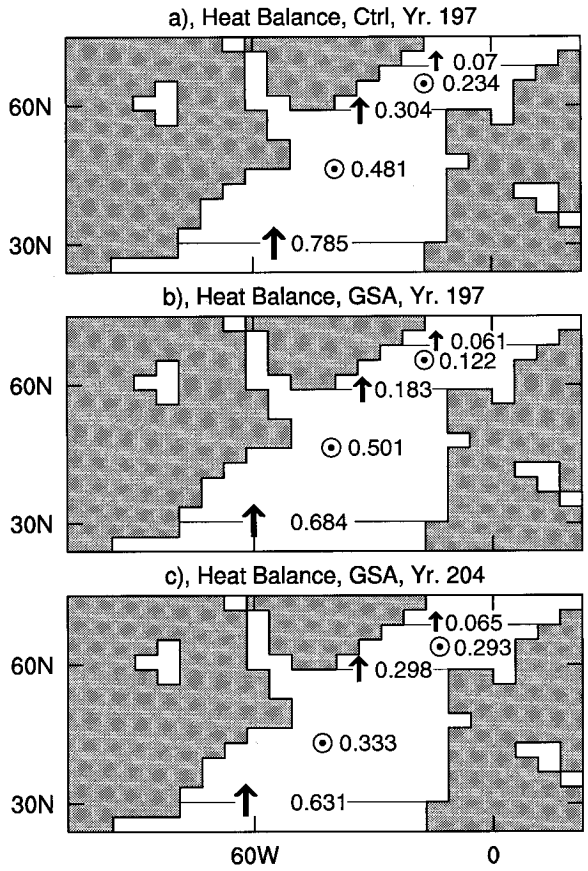

FIG. 13. Heat balance (a) at year 197 of the control run, (b) at year 197 of the GSA experiment, and (c) at year 204 of the GSA experiments.

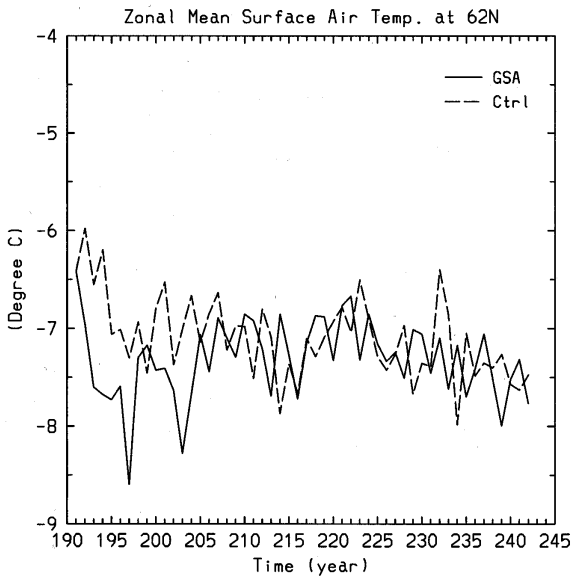

FIG. 14. Time evolution of the zonal mean surface air temperature (°C) at 62°N.

a minimum at year 197 but that near the equator at year 207, a lag of about 10 yr. This indicates that there are basin-wide impacts and differing timescales for the response involved.

The latitudinal lag in the response of oceanic heat transport has substantial influence on the fate of surface temperature anomalies in the high and midlatitudes. Figure 13 shows the heat balance (a) at year 197 of the control run, (b) at year 197 of the GSA run, and (c) at year 204 of the GSA run. The balance at year 197 of the control run represents a typical normal condition. At the latitudes from 30° to 58°N (hereafter referred to as midlatitude region) and from 58° to 68°N (hereafter referred to as high-latitude region), the ocean loses heat to the atmosphere at a rate of 0.481 PW and 0.234 PW on annual average, respectively. In the GSA run, by year 197 the freshening has caused a decrease in poleward heat transport and a decrease in heat loss (from 0.234 to 0.122 PW) in the high-latitude region (Fig. 13b). In the midlatitude region, although the heat transport at the northern boundary has decreased from 0.304 to 0.183 PW, because of the lag, the decrease in the southern boundary is not as much, from 0.785 to 0.685 PW. This means that there is less net heat transported from the midlatitude to the high-latitude region. This leads to an accumulation of heat in the midlatitude region. Consequently, the temperature rises and heat loss increases. The warm temperature anomaly penetrates to about 500-m depth [Fig. 4c(i)].

The temperature contrast between the midlatitude and high-latitude regions increases. This acts to increase the north–south pressure gradient, which plays a role in the recovery of the NADWF upon the cessation of the imposed freshening. Further, these anomalies are situated mainly over the convection region and will in turn affect the ocean circulation. These points will be discussed in section 4.

e. The atmospheric response

We concentrate on time-dependent responses of atmospheric fields influenced by forced oceanic changes and on atmospheric responses averaged over a 5-yr period centered at the time when the NADWF is at a minimum.

1) SURFACE TEMPERATURE

Figure 14 shows the time evolution of annual average of zonal mean surface air temperature at 62°N. A clear signal is seen. Surface air temperature drops as SST cools, creating a greater equator to pole contrast of temperature. This leads to an increase in the atmospheric heat transport, which occurs through the negative feedback between the atmospheric and oceanic heat transport. However, a net cooling occurs. A plot of annual mean surface air temperature (2-m temperatures) anomalies (GSA − Control) at year 197 shows that the response of this field is global in scale, with a stronger

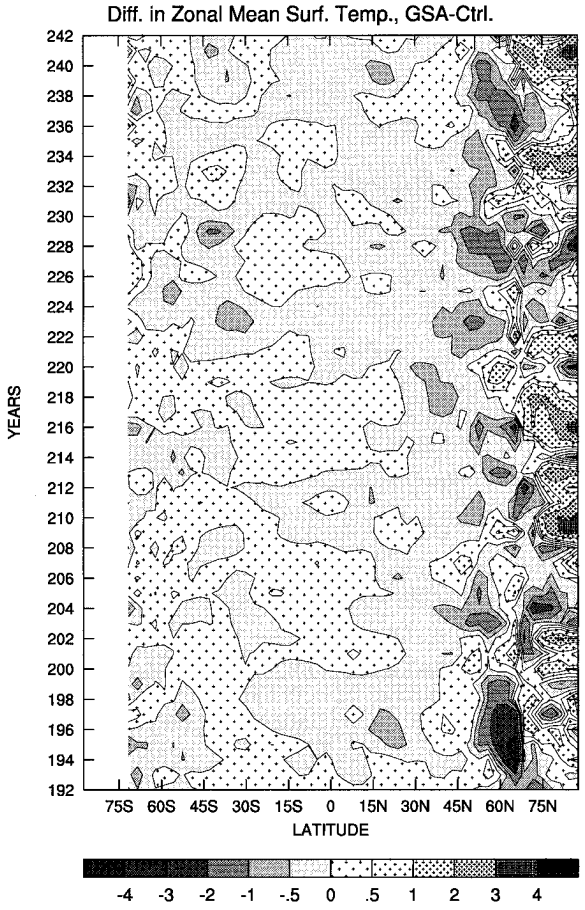

FIG. 15. Time–latitude plot of the difference (GSA—Control) in DJF zonal mean surface temperature in the Atlantic Ocean (including the whole Arctic Ocean).

signal in mid- to high latitudes than in the Tropics. When compared to Fig. 5, the change of surface air temperature over the ocean follows that of SST except over sea ice, which reduces the heat exchange between the water surface and the overlying air. Over the land, a strong cooling occurs over the northern part of Eurasia, the western part of North America, and south of Greenland. A mild warming takes place over the eastern part of North America, northeastern Greenland, and the central North Atlantic.

The atmospheric response shows marked difference over different seasons; during the boreal winter, the responses exhibit the largest signal. Therefore, hereafter the description of the atmospheric responses focuses on the mean of the northern winter season [December, January, and February (DJF)]. Zonal mean over the Atlantic Ocean (including the whole Arctic Ocean) of the mean DJF temperature changes are calculated for the entire length of the experiment and are shown in Fig. 15. Throughout the experiment there are occurrences of cooling events lasting for several years. However, during the first 9 yr of the GSA experiment, zonal mean temperatures decrease by up to 4° at 52°–68°N latitude band and increases moderately south of it. During the following 5–7 yr the anomalies at 52°–68°N latitude band revert signs.

To examine the geographic distributions of the northern winter anomalies, we have calculated the difference in climatological fields by averaging over the period between year 195 and year 199 (centered at around the time when the North Atlantic overturning is at a minimum, see Fig. 3a). The field for surface temperature changes is shown in Fig. 16. Cooling occurs in seas around Greenland and Labrador, and adjacent lands, and over the extended sea ice cover in the region. A moderate cooling also occurs in Scandinavia, western Europe, the Middle East, and far eastern Russia. However, there is moderate warming over Alaska, western Siberia, northern Greenland, and northern Greenland–Barents Seas. By contrast, the summer surface temperature changes (figure not shown) are more confined to the region of imposed freshening.

To evaluate effects of the imposed freshening on temperature change at different timescales, we calculate temperature difference between the GSA experiment

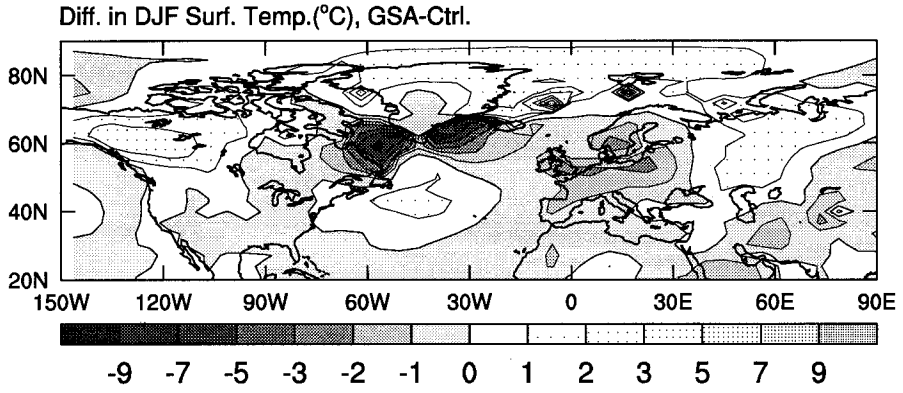

FIG. 16. Difference (GSA—Control) in DJF mean surface temperature averaged over a 5-yr period from year 195 to year 199.

and the control run and divide it by the standard deviation of the control run. We also calculate interannual standard deviations of surface temperature from each experiment and derive the ratio of standard deviation between the GSA experiment and the control run. These two measures combined indicate whether the forced signal is significant over the chaotic variations at timescales within which these calculations are performed. The calculations are carried out using fields covering the period from year 195 to year 199, from year 192 to year 201, from year 192 to year 211, and over the entire length of experiment (from year 192 to year 242). The results (figures not shown) are described below. At the timescale of 50 years, a significant cooling (i.e., more than several standard deviations) occurs only in an area of imposed freshening. At the timescale of 20 yr, a significant cooling extends eastward and covers most of Norwegian Sea, Scandinavia, and British Isles, suggesting that the effect of a GSA event is long lasting. At the 10-yr timescale the extent of cooling is similar to that of the 20-yr case, but the cooling is more pronounced. At the 5-yr timescale, strong cooling extends from eastern Canada through the high-latitude North Atlantic to western Europe, and the Mediterranean and subtropical Atlantic, whereas a significant warming occurs over the midlatitude North Atlantic, Alaska, north Greenland, Greenland–Barents Seas, and western Siberia.

2) Atmospheric circulation

One direct result of the surface temperature changes is the stabilization of the atmosphere over colder ocean waters of the North Atlantic. Figure 17a shows changes in sea level pressure. We see a reduced intensity of the Icelandic low (which dominates most of the North Atlantic Ocean) and increased pressures over eastern North America, Greenland, and western Siberia. A compensating deepening of the Aleutian low and a weakening of the influence of Azores high over western Europe are also evident. Figure 17b shows the changes in geopotential height at 500 mb. A dominant feature is a sharp increase in heights over the midlatitude North Atlantic, western Siberia, and western coast of Canada. This is consistent with the surface warming discussed above. Another feature is the decrease over western Europe, also consistent with the surface cooling there. Changes in the prevailing circulation (Fig. 18) at 850 hPa show a reduction in the zonal component over the midlatitude North Atlantic of up to 3 m s^{-1} giving rise to reduced westerlies. There is also a reduction in the meridional component over the eastern North Atlantic. The reduction leads to a southward shift of westerlies from Scandinavia to western Europe and the Mediterranean, resulting in reduced westerlies over northern Eurasia. Another feature is a positive correlation between the strength of westerlies and the Atlantic trade winds. This is consistent with observation (see Wallace and Gutzler 1981, 811).

3) The North Atlantic Oscillation index

The atmospheric circulation over the North Atlantic is affected by changes in the location of the climatological mean jet stream, and this is strongly evident in observational data (Wallace and Gutzler 1981; Lamb and Peper 1987). A common measure of such changes is the North Atlantic oscillation (NAO) index (Hurell 1995, 1996). NAO is characterized by seasonal variations in the regional sea level pressure gradient, midlatitude westerlies, sea surface temperature, and the climate of the adjacent continents. A climate state with a positive NAO index is generally accompanied by an anomalously strong Azores high and a deep Icelandic low. Therefore, the westerlies over the Atlantic Ocean are stronger, allowing warm surface ocean water and mild air masses to advect northeastward across the Atlantic toward Europe and the eastern Arctic. By contrast, a state with negative NAO index is associated with pressure gradients anomalously weak. Therefore, the Icelandic low is displaced toward Newfoundland, while atmospheric blocking patterns occur in the flow aloft and polar anticyclones extend southward to the eastern Atlantic and Europe, and winters in the northern and western Europe are very cold. It has been argued (Barlow et al. 1993; Harrison et al. 1996) that a state with a negative NAO index is a good example of prevailing circulation during the Little Ice Age and the Last Glacial Maximum.

To examine the time-dependent behavior of NAO index in both the control run and the GSA experiment, we have calculated NAO index following Hurell (1995) for both runs and the results are plotted in Fig. 19. It shows pronounced changes in the wintertime atmospheric circulation in the GSA experiment from the control run. The raw data curves (without filtering) show irregular oscillations with amplitude and frequency similar to those observed by Hurell (1995, see his Fig. 1). There are also episodes in both runs where NAO index is negative for several years. These may represent cases of self-generated oscillations of the coupled system. However, during the first 10 yr or so of the GSA experiment, NAO index undergoes a series of fluctuations with trends toward negative values. As a result, NAO index changes from positive in the control run to negative in the GSA experiment during the first 10 yr of the GSA experiment. Thereafter NAO index recovers toward positive values.

The strength of the moisture-bearing westerlies (toward western Europe) over the midlatitude North Atlantic Ocean is determined by whether NAO is negative or positive (Lamb and Peper 1987; Hurell 1995). Hurell has shown that the precipitation in Europe is related to different NAO states. During winters with positive NAO values, much of central and southern Europe and the

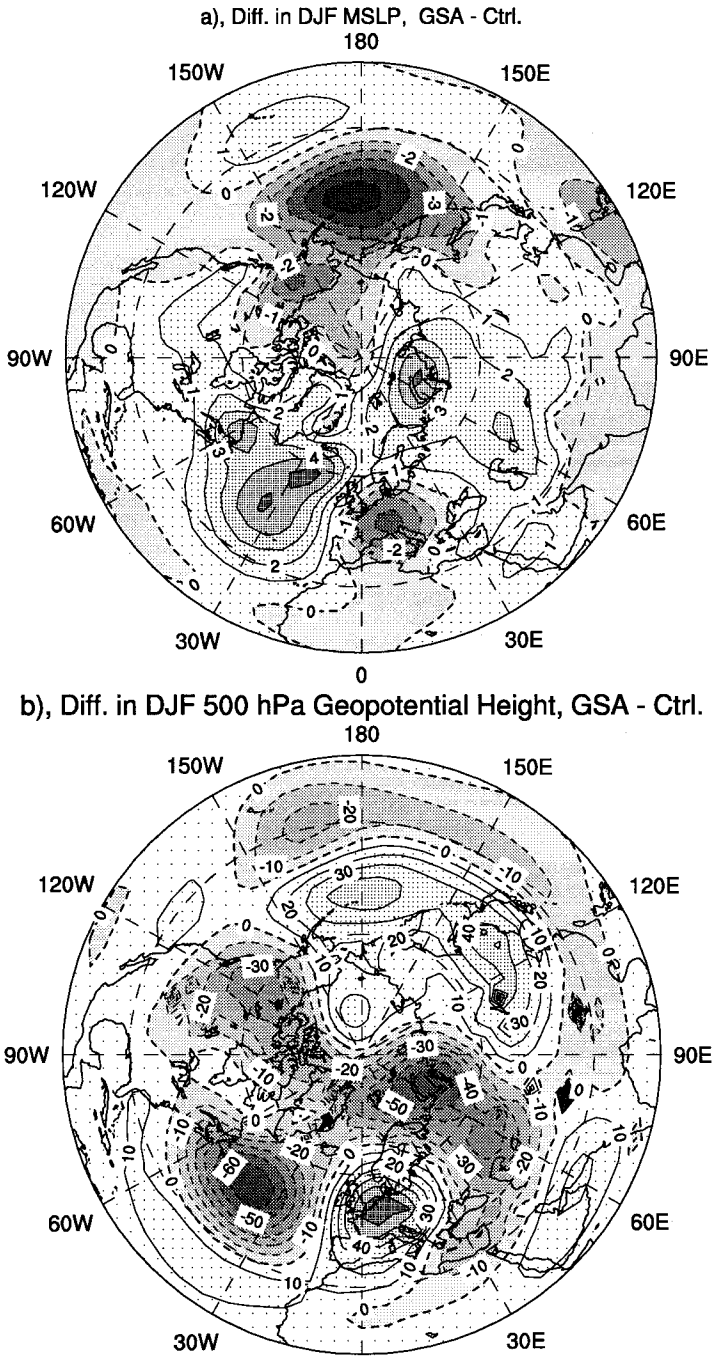

FIG. 17. Difference (GSA—Control) in DJF mean of (a) mean sea level pressure and (b) geopotential height at 500 hPa, both averaged over a 5-yr period from year 195 to year 199. Contour interval is 1 hPa for (a) and 10 hPa for (b). Both plots cover latitudes from 10° to 90°N.

Mediterranean have drier conditions and in the meantime there is an increased convergence of moisture flux over Iceland and Scandinavia, and vice versa. To see if the model produces this feature, we have examined moisture balance over western Europe (Fig. 20). The difference in E − P shows a drier condition over Iceland–Scandinavia and the Mediterranean but a wetter condition over western Europe and the southeastern coast of Greenland. This is consistent with Hurell's findings. The difference between the GSA experiment and the control run in annual average of E − P indicates an increased moisture supply to the eastern coast of Green-

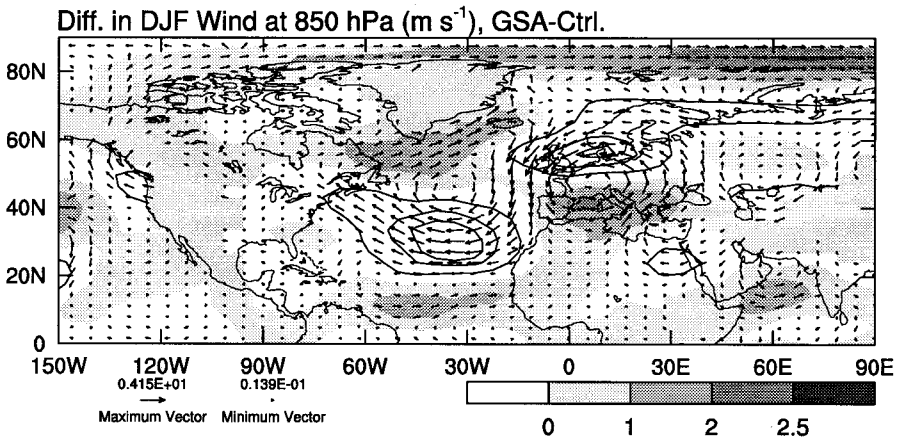

FIG. 18. Difference (GSA—Control) in DJF mean of wind vectors at 850 HPa, averaged over a 5-yr period from year 195 to year 199. Superimposed on the wind vectors are contours of the zonal component with contour interval at 1, 2, and 2.5 m s^{-1}; positive contours are shaded and negative ones have contour line drawn.

land and Iceland, eastern Canada, and Scandinavia, leading to an increased snow accumulation, a feature characteristic of little-ice-ages-like episodes. The increased snow accumulation over Scandinavia and western Europe, despite decreased moisture supply, is due to the colder conditions in winter.

4. The response upon cessation of the imposed freshening

a. The recovery of NADWF

Approximately 1 yr after the imposed freshening ceases, the overturning, surface temperature, surface salinity, and surface density at 62°N start to recover (Fig. 3). The recovery of the overturning is slower than that of the surface salinity and temperature. The surface temperature appears to have fully recovered by year 210, but later (from year 220) drops below the value of the control run, suggesting that the recovery is an overshoot above a new mean value. Throughout the course of recovery, the surface salinity is lower than that of the control run, although with a similar overshoot. This low salinity leads to generally lower densities than in the control run.

The cooling in the high latitude and the warming in the low-latitude region established during the imposed freshening set up favorable conditions for the recovery of NADWF upon the cessation of the imposed freshening. On the one hand, the cool water contributes to an increase in density once the freshening is removed. This can be seen from Fig. 3d (the fine dashed curve), which shows that without the cooling surface density would be much lower. On the other hand, the enhanced temperature contrast between the midlatitude and high latitude increases the north–south pressure gradient, contributing to the recovery of NADWF.

A similar mechanism is found to play a significant role in the recovery of NADWF in double CO_2 experiments reported by Manabe and Stouffer (1993, 1994) and Bryan and Spelman (1985). In their studies, the surface warming penetrates into the thermocline of the subtropics during the process of the initial weakening of the thermohaline circulation. This is caused not only by the atmospheric warming, but also by the weakening of the vertical advection at low latitudes of relatively cold water because of the reduced NADWF. At high latitudes, although warming occurs, it is not as strong, since less heat is advected from the Tropics as NADWF weakens. This enhances the north–south pressure gradient, similar to the situation we have described above, which is favorable to recovery upon the cessation of atmospheric warming. The only difference between their case and this one is that in our case the scale is not as large and the intensity is not as strong.

The recovery has considerable phase differences at different latitudes. For example, by year 204, although the overturning at high latitude has recovered somewhat, NADWF outflow across the equator is still weakening [Figs. 4a(i) and 4a(ii)]. The recovery of the outflow commences at year 215. In the midlatitude region (that is, from 30° to 58°N), where warming occurs during the freshening, a substantial cooling has started by year 204 [Fig. 5b(ii)]. The salinity in the midlatitudes behaves somewhat differently: high salinity persists and moves slowly northward. In the meantime, the high-latitude low salinity anomaly rotates in a clockwise direction into the midlatitude region [Fig. 5b(i)]. By year 215 the high salinity has almost disappeared. This behavior leads to a positive density anomaly that moves northward across the midlatitude region and penetrates to depth as the overturning recovers.

It is the dominance of the negative feedbacks over the positive feedback of the system that enables the small weakening of NADWF during the initial fresh-

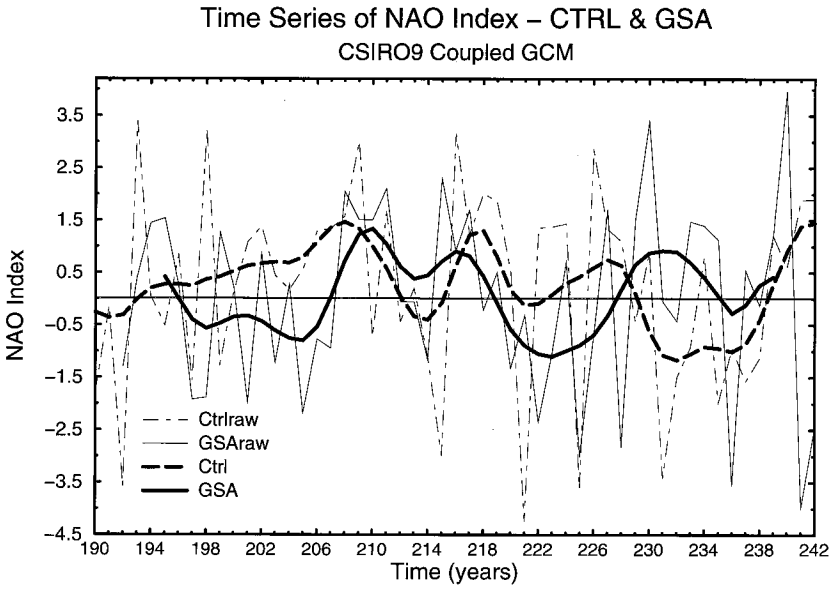

FIG. 19. Winter (from December to March) index of the North Atlantic Oscillation for both the GSA experiment and the control run. The index is based on the difference in normalized mean sea level pressure between model grids over Lisbon and over Iceland, and is constructed in the same way as the Fig. 1 in the Hurell (1995) study. The thick lines represent smoothed curves with fluctuations on timescales of less than 4 yr removed by a low-pass filter with seven weights (1, 3, 5, 6, 5, 3, and 1).

ening and eventual recovery of it. However, the role of feedbacks is different from that during the initial weakening of NADWF (during years 192–197). For example, in the region with imposed freshening, as NADWF recovers, convective activity resumes (Fig. 6). Through the negative feedback between temperature and overturning, heat transport increases and the surface temperature rises [Figs. 5a(ii) and 5b(ii)]. The evaporation rate returns abruptly to near normal conditions (Fig. 7), contributing to the increase in surface salinity (thereafter the signal may not be significant). On the other hand, sea ice melts rapidly (Figs. 9 and 10) and the associated freshwater input acts to decrease surface salinity. When these feedbacks are taken together, the net effect is that high-latitude salinity increases. This enhances the thermohaline circulation, which in turn accompanies an intensification of the increase in surface salinity.

The overturning associated with NADWF is reestablished by year 215. In fact, the density (fine dash) curve of Fig. 3d shows that even in the absence of the initial cooling, and even if NADWF is weakened further during the freshening, NADWF will still recover. This re-

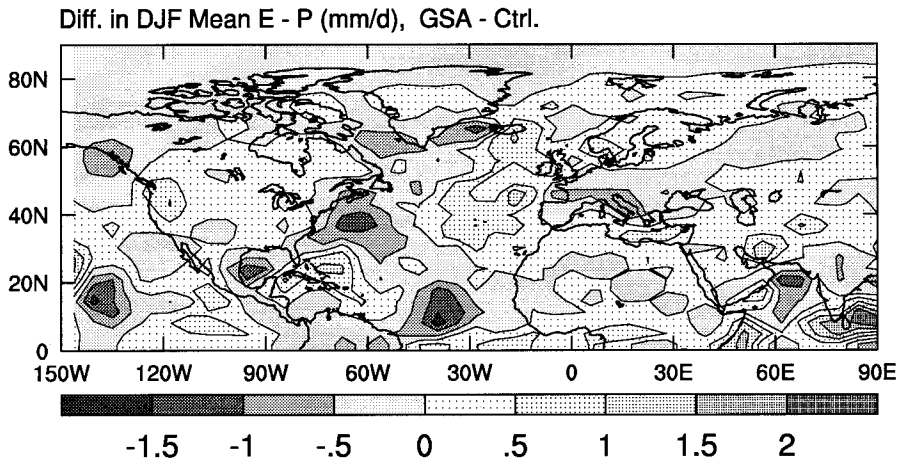

FIG. 20. Difference (GSA—Control) in DJF mean of E − P balance averaged over a 5-yr period from year 195 to year 199.

covery underscores the resilience of the thermohaline circulation. It also implies that the current thermohaline circulation is strongly dominated by thermal circulation and the associated negative feedbacks. This point is supported by the presence of a number of overshoots, which are typical features of an inertial system dominated by negative feedbacks (Rahmstorf and Willebrand 1995; Cai and Godfrey 1995). Once the thermohaline circulation recovers, the large-scale barotropic (Fig. 11) and baroclinic circulation gradually recover to near that of the control run.

The atmospheric response to the cessation of the imposed freshening is much more rapid than the oceanic counterpart. For example, at 62°N the atmospheric moisture transport (Fig. 7), the ice thickness (Fig. 9), the surface albedo, and the atmospheric heat transport (Fig. 10) all return to near normal conditions by year 200. However, as discussed in section 3e, the GSA-like event has lasting effect on the climate of the Atlantic and adjacent continents.

b. The continued cooling in the midlatitude Atlantic

Upon the cessation of freshening, a cooling in midlatitudes persists to about year 230. This cooling is a direct consequence of the lag of the response in poleward heat transport at lower latitudes. For example, by year 204 the heat transport in the high latitudes has almost recovered. In the midlatitude region, although the transport at the northern boundary has almost recovered (Fig. 13c), the transport at the southern boundary is still weakening. This leads to a heat deficit in the region and, therefore, a drop in temperature and a reduction in heat loss (from 0.481 to 0.338 PW). The cooling penetrates to depth, even to the high-latitude deep ocean. The cold anomalies last until about year 230, when the heat transport at the southern boundary has recovered and the water has warmed to a temperature comparable to that of the control run. The development of the negative temperature anomaly has contributed to a positive density anomaly [Fig. 5b(iii)], which tends to intensify the convective activity in the region (Fig. 6c). This in turn favors the persistence of the positive salinity anomaly there (Fig. 5b).

5. Summary

During the 1970s we experienced a GSA event. Such an event may occur again. The GSA event is a natural occurrence of the coupled oceanic–atmospheric–sea ice system and is difficult to simulate. However, it is possible to study the response of a coupled system to a similar freshening so as to understand the processes involved.

Many previous studies into this subject used ocean-only models. These models exclude many of the important oceanic feedback processes and those included are time and spatially independent. Further atmospheric feedbacks and atmosphere–ocean interactions are excluded altogether. The present study uses a coupled ocean–atmosphere model. In this coupled model, all the major ocean feedbacks are present, and they are a function of time and space, determined by the coupled model dynamics. The use of a coupled model also allows atmospheric feedbacks and ocean–atmosphere interactions.

In the present study, the imposed North Atlantic high-latitude freshening lasts for 5 yr with a total salt deficit equivalent to about eight times the observed GSA (Dickson 1988) during the late 1960s and early 1970s. The thermohaline circulation associated with the NADWF first weakens but recovers within 20 yr after the imposed freshening flux is removed. We explored several important aspects that were not examined in previous studies. These include the temporal and spatial scale of the response, the time-dependent impact on the large-scale circulation, and the process that leads to the recovery.

As the freshening proceeds, initially, only the part of the conveyor-belt circulation near the imposed freshening slows down; the circulation in regions remote from the imposed freshening proceeds as usual. The slow-down is then gradually felt by the southern part of the conveyor belt. In this way, the effects of the salinity anomaly are gradually transmitted from high latitude to the entire Atlantic Ocean, against the flow of the conveyor belt. For example, at year 197, 1 yr after the imposed freshwater anomaly is removed, the heat transport at 62°N has reached a minimum but at 30°N the response to the freshening has just started. The delay is about 10 yr between 62°N to the equator. In the midlatitude (from 30° to 58°N) region, the lag causes a warming during the initial weakening and a cooling during the recovery. Since the conveyor belt merely slows down, rather than stops altogether, and since it returns to its full strength upon the cessation of the freshening, throughout the entire episode, the conveyor belt circulation operates.

The changes in the thermohaline circulation significantly modify the large-scale North Atlantic circulation. In particular, the strength of baroclinic flows associated with the conveyor belt circulations reduces as the convection at high latitudes weakens. Further, the barotropic Gulf Stream weakens by about 18%. This influence on the Gulf Stream is supported by results inferred from hydrographic data prior to and during the GSA event of the 1970s (Greatbatch et al. 1991).

As the overturning weakens, the high-latitude surface temperature decreases through negative feedback between temperature and overturning. Once the imposed freshwater anomaly is removed, this cooling acts to increase the surface density. Further, the warming in the midlatitudes and the cooling in the high latitudes increase the north–south pressure gradient. These conditions, which are set up during the initial weakening of NADWF, then contribute to the final recovery. Once the

recovery is initiated, it is aided by the ocean positive feedbacks.

Modifications of the thermal structure of the surface ocean lead to changes in the atmospheric circulation, in particular, a weakening of the westerlies over the midlatitude North Atlantic and a southward shift over western Europe. NAO index under imposed freshening is negative, which is consistent with observational evidence, and the associated climate changes are similar to observed ones during negative phase of NAO.

The recovery of the thermohaline circulation suggested that it is resilient in a coupled model environment. This is reflected in a series of overshoots during the recovery. This high stability of the thermohaline circulation in a coupled system is also supported by other work. Manabe and Stouffer (1995) found that even under an imposed freshening over a broader region and with a magnitude comparable to the pre-Younger Dryas discharge, the NADWF still recovers. As in Manabe and Stouffer's model flux corrections are used. It is not entirely clear to what extent they affect the stability of the thermohaline circulation. Nevertheless, the time-dependent response at different lag and at different location, the dipole structure of the SST response with cooling in the sinking region and warming south of it, and the significant reduction in the Gulf Stream followed by a subsequent recovery are intriguing. Furthermore, our coupled model reproduced many observed atmospheric responses associated with a freshening event. We believe that observations of these features should provide information as to whether or not a GSA event is under way.

Acknowledgments. This work is supported by a core greenhouse grant from the Australian Department of Environment, Sport, and Territories. J.S. is supported by a dedicated NGAC grant. Many members of the CSIRO Climate Modeling Program contributed to the development of the coupled model. We thank B. Hunt for his continuing support, P. G. Baines, K. Walsh, and I. G. Watterson for interesting discussion, and reviewers for constructive comments. Harvey Davies provided the plotting routines. The computations were carried out on the CSIRO CRAY-YMP4E/464.

REFERENCES

Barlow, L. K., J. W. C. White, R. G. Barry, J. C. Rogers, and P. M. Grootes, 1993: The North Atlantic Oscillation signature in deuterium and deuterium excess signals in the Greenland Ice Sheet Project 2 Ice Core, 1840–1970. *Geophys. Res. Lett.,* **20,** 2901–2904.

Broecker, W. S., 1991: The great conveyor belt. *Oceanography,* **4,** 79–89.

——, D. M. Peteet, and D. Rind, 1985: Does the ocean–atmosphere system have more than one stable mode of operation? *Nature,* **315,** 21–26.

Bryan, F., 1986: High-latitude salinity effects and interhemispheric thermohaline circulation. *Nature,* **323,** 301–304.

Bryan, K., 1969: A numerical method for the study of the circulation of the World Ocean. *J. Comput. Phys.,* **4,** 347–376.

——, and M. J. Spelman, 1985: The ocean's response to a CO_2-induced warming. *J. Geophys. Res.,* **90,** 11 679–11 688.

Cai, W., 1994: Circulation driven by observed surface thermohaline fields in a coarse resolution ocean general circulation model. *J. Geophys. Res.,* **99,** 10 163–10 181.

——, 1995: Interdecadal variability driven by mismatch between surface flux forcing and oceanic freshwater/heat transport. *J. Phys. Oceanogr.,* **25,** 2643–2666.

——, 1996: The stability of NADWF under mixed boundary conditions with an improved diagnosed freshwater flux field. *J. Phys. Oceanogr.,* **26,** 1081–1087.

——, and S. Godfrey, 1995: Surface heat flux parameterizations and the variability of thermohaline circulation. *J. Geophys. Res.,* **100,** 10 679–10 692.

——, and R. J. Greatbatch, 1995: Compensation for the NADW outflow in a global ocean general circulation model. *J. Phys. Oceanogr.,* **25,** 226–241.

——, and P. G. Baines, 1996: Interactions between thermohaline and wind-driven circulations and their relevance to the dynamics of the Antarctic Circumpolar Current, in a coarse resolution global OGCM. *J. Geophys. Res.,* **101,** 14 073–14 093.

——, and P. C. Chu, 1996: Ocean climate variability and drift due to a change in thermal damping. *J. Climate,* **9,** 2821–2833.

Chappell, J., and J. Syktus, 1996: Paleoclimatic modeling: A western Pacific perspective. *Climate Change: Developing Southern Hemisphere Perspectives,* T. W. Giambelluca and A. Henderson-Sellers, Eds., John Wiley and Sons, 175–193.

Danabasoglu, G., and J. McWilliams, 1995: Sensitivity of the global ocean circulation to parameterizations of mesoscale tracer transports. *J. Climate,* **8,** 2967–2987.

Dickson, R. R., J. Meincke, S. A. Malmberg, and A. L. Lee, 1988: "Great Salinity Anomaly" in the northern North Atlantic, 1968–82. *Progress in Oceanography,* Vol. 20, Pergamon Press, 103–151.

Flato, G. M., and W. D. Hibler, 1990: On a simple sea-ice dynamics model for climate studies. *Annu. Glaciol.,* **14,** 72–77.

Gleckler, P. J., and Coauthors, 1995: Cloud-radiative effect on implied oceanic energy transports as simulated by atmospheric general circulation models. *Geophys. Res. Lett.,* **7,** 791–794.

Gordon, A. L., 1986: Interocean exchange of thermocline water. *J. Geophys. Res.,* **91,** 5037–5046.

Gordon, H. B., and S. P. O'Farrell, 1997: Transient climate change in the CSIRO coupled model with dynamics sea-ice. *Mon. Wea. Rev.,* **125,** 875–907.

Greatbatch, R. J., A. F. Fanning, A. D. Goulding, and S. Levitus, 1991: A diagnosis of interpentadal circulation changes in the North Atlantic. *J. Geophys. Res.,* **96,** 22 009–22 023.

Haney, L. R., 1971: Surface boundary condition for ocean circulation models. *J. Phys. Oceanogr.,* **1,** 241–248.

Harrison, S. P., G. Yu, and P. E. Tarasov, 1996: Late quaternary lake-level record from Northern Eurasia. *Quat. Res.,* **45,** 138–159.

Hellerman, S., and M. Rosenstein, 1983: Normal monthly wind stress over the World Ocean with error estimates. *J. Phys. Oceanogr.,* **13,** 1093–1704.

Holland, W. R., 1973: Baroclinic and topographic influences on the transport in western boundary currents. *Geophys. Fluid Dyn.,* **4,** 187–210.

Hunt, B. G., H. B. Gordon, and H. L. Davies, 1995: Impact of the greenhouse effect on sea-ice characteristics and snow accumulation in the polar regions. *Int. J. Climatol.,* **15,** 3–23.

Hurell, J. W., 1995: Decadal trend in the North Atlantic Oscillation: Regional temperatures and precipitation. *Science,* **269,** 676–679.

——, 1996: Influence of variations in extratropical wintertime teleconnections on Northern Hemisphere temperature. *Geophys. Res. Lett.,* **23,** 665–668.

Keigwin, L. D., and G. A. Jones, 1994: Western North Atlantic evidence for millennial-scale changes in ocean circulation and climate. *J. Geophys. Res.,* **99,** 12 397–12 410.

Kowalczyk, E. A., J. R. Garratt, and P. B. Krummel, 1991: A soil-canopy scheme for use in a numerical model of the atmosphere—1D stand-alone model. CSIRO Division of Atmospheric Research Tech. Paper 23, 56 pp. [Available from CSIRO Division of Atmospheric Research, 107-121 Station St., Aspendale, Vic. 3195, Australia.]

——, ——, and ——, 1994: Implementation of a soil-canopy scheme into the CSIRO GCM—Regional aspects of the model response. CSIRO Division of Atmospheric Research Tech. Paper 32, 59 pp. [Available from CSIRO Division of Atmospheric Research, 107-121 Station St., Aspendale, Vic. 3195, Australia.]

Lamb, P. J., and R. A. Peppler, 1987: North Atlantic Oscillation: Concept and an application. *Bull. Amer. Meteor. Soc.,* **68,** 1218–1225.

Levitus, S., 1982: *Climatological Atlas of the World Ocean.* NOAA Prof. Paper 13, U.S. Govt. Printing Office, 173 pp.

——, 1989a: Interdecadal variability of temperature and salinity at intermediate depths of the North Atlantic Ocean, 1970–1974 versus 1955–1959. *J. Geophys. Res.,* **94,** 6091–6131.

——, 1989b: Interdecadal variability of salinity at upper 15 m of the North Atlantic Ocean, 1970–1974 versus 1955–1959. *J. Geophys. Res.,* **94,** 9679–9685.

——, 1989c: Interdecadal variability of temperature and salinity in the deep North Atlantic, 1970–1974 versus 1955–1959. *J. Geophys. Res.,* **94,** 16 125–16 131.

Manabe, S., and R. J. Stouffer, 1988: Two stable equilibria of a coupled ocean–atmosphere model. *J. Climate,* **1,** 841–866.

——, and ——, 1993: Century-scale effects of increased atmospheric CO_2 on the ocean–atmosphere system. *Nature,* **364,** 215–218.

——, and ——, 1994: Multiple century response of a coupled ocean–atmosphere model to an increase in atmospheric carbon dioxide. *J. Climate,* **7,** 5–23.

——, and ——, 1995: Simulation of abrupt climate change induced by freshwater input to the North Atlantic Ocean. *Nature,* **378,** 165–167.

Marotzke, J., 1994: Ocean models in climate problems. *Ocean Progress in Climate Dynamics: Global and Mediterranean Examples,* P. Malanatte-Rizzoli and A. R. Robinson, Eds., Kluwer Academic Publishers, 79–109.

——, and J. Willebrand, 1991: Multiple equilibria of the global thermohaline circulation. *J. Phys. Oceanogr.,* **21,** 1372–1385.

——, and P. Stone, 1995: Atmospheric transports, the thermohaline circulation, and flux adjustments in a simple coupled model. *J. Phys. Oceanogr.,* **25,** 1350–1364.

McGregor, J. L., H. B. Gordon, I. G. Watterson, M. R. Dix, and L. D. Rotstayn, 1993: The CSIRO 9-level atmospheric general circulation model. CSIRO Division of Atmospheric Research Tech. Paper 26, 89 pp. [Available from CSIRO Division of Atmospheric Research, 107-121 Station St., Aspendale, Vic. 3195, Australia.]

Moore, A. M., and C. J. C. Reason, 1993: The response of a global OGCM to climatological surface boundary conditions for temperature and salinity. *J. Phys. Oceanogr.,* **23,** 300–328.

——, and H. B. Gordon, 1994: An investigation of climate drift in coupled atmosphere–ocean–sea ice model. *Climate Dyn.,* **10,** 81–95.

Nakamura, M., P. Stone, and J. Marotzke, 1994: Destabilization of the thermohaline circulation by atmospheric eddy transports. *J. Climate,* **7,** 1870–1882.

Power, S. B., A. M. Moore, D. A. Post, N. R. Smith, and R. Kleeman, 1994: Stability of North Atlantic deep water formation in a global ocean general circulation model. *J. Phys. Oceanogr.,* **24,** 904–916.

Rahmstorf, S., and J. Willebrand, 1995: The role of temperature feedback in stabilizing the thermohaline circulation. *J. Phys. Oceanogr.,* **25,** 778–805.

Rintoul, S. R., 1991: South Atlantic interbasin exchange. *J. Geophys. Res.,* **96,** 2675–2692.

Saravanan, R., and J. McWilliams, 1995: Multiple equilibrium, natural variability, and climate transitions in an idealized ocean–atmosphere model. *J. Climate,* **8,** 2296–2323.

Schneider, E., 1996: Flux corrections and the simulation of changing climate. *Ann. Geophys.,* **14,** 336–341.

Semtner, A. J., 1976: A model for the thermodynamic growth of sea ice in numerical investigations of climate. *J. Phys. Oceanogr.,* **6,** 379–389.

——, and R. M. Chervin, 1988: A simulation of the global ocean circulation with resolved eddies. *J. Geophys. Res.,* **93,** 15 502–15 522.

Stommel, H., 1961: Thermohaline convection with two stable regimes of flow. *Tellus,* **13,** 224–230.

Stone, P. H., 1978: Constraints on dynamical transports of energy on a spherical planet. *Dyn, Atmos. Oceans,* **2,** 123–139.

Syktus, J., H. Gordon, and J. Chappell, 1994: Sensitivity of a coupled atmosphere-dynamic upper ocean GCM to variations of CO_2, solar constant, and orbital forcing. *Geophys. Res. Lett.,* **21,** 1599–1602.

Wallace, J. M., and D. S. Gutzler, 1981: Teleconnections in the geopotential height field during the Northern Hemisphere winter. *Mon. Wea. Rev.,* **109,** 784–812.

Walsh, J. E., and W. L. Chapman, 1990: Arctic contribution to upper-ocean variability in the North Atlantic. *J. Climate,* **3,** 1725–1473.

Watterson, I. G., M. R. Dix, H. B. Gordon, and J. L McGregor, 1995: The CSIRO9 AGCM and its equilibrium present and doubled CO_2 climates. *Aust. Meteor. Mag.,* **44,** 111–125.

Willebrand, J., 1993: Forcing the ocean by heat and freshwater fluxes. *Energy and Water Cycles in the Climate System,* E. Raschke and D. Jacob, Eds., NATO ASI Series, Vol. 15, Springer-Verlag, 215–223.

Wright, D. G., and T. F. Stocker, 1991: A zonally averaged ocean model for the thermohaline circulation. Part I: Model development and flow dynamics. *J. Phys. Oceanogr.,* **21,** 1713–1724.

Yang, J., and D. Neelin, 1993: Sea-ice interaction with the thermohaline circulation. *Geophys. Res. Lett.,* **20,** 217–220.

Zhang, S., C. A. Lin, and R. J. Greatbatch, 1995: A decadal oscillation due to the coupling between an ocean circulation model and a thermodynamics sea-ice model. *J. Mar. Res.,* **53,** 79–106.